Application of Automatic Differentiation in Electromagnetic Dosimetry – Assessment of the Absorbed Power Density in the mmWave Frequency Spectrum

Ante Lojić Kapetanović*, Dragan Poljak†
Faculty of Electrical Engineering, Mechanical Engineering and Naval Architecture
University of Split
Split, Croatia
*alojic00@fesb.hr, †dpoljak@fesb.hr

***Abstract*—This paper introduces the concept of automatic differentiation in the evaluation of the absorbed power density in the mmWave frequency spectrum for the new generation of mobile telecommunication technology. Automatic differentiation has been shown to be far superior over numerical differentiation by means of speed and accuracy. To demonstrate the full capacity of the proposed method, a comprehensive analysis of computing the absorbed power density on the surface of irradiated human skin in various configurations is presented.**

***Index Terms*—automatic differentiation, absorbed power density, computational electromagnetic dosimetry, 5G telecommunication technology**

I. Introduction

The accurate assessment of human exposure to radiated electromagnetic fields (EMFs) is of particular importance in the computational electromagnetic dosimetry, whereby through various independent guidelines and standards, basic restrictions are defined for the safe human to EMF interaction. International guidelines [1] and standards [2] have recently undergone comprehensive revisions, primarily with regards to frequencies of the mmWave frequency spectrum, given developments and recent deployment of the 5G telecommunication technology worldwide [3]. Frequencies of interest range from 100 MHz to 300 GHz, thus covering the entirety of radio-frequency spectrum. Up to 3 GHz, the specific absorption rate (SAR) averaged over a 1 g or 10 g cube of tissue is defined as the basic restriction. Above 6 GHz, the absorbed or epithelial power density (APD) averaged over the surface area of 1 cm^2 or 4 cm^2, corresponding to the area of the exposed surface of 1 g or 10 g cube of tissue [4], respectively, is defined as the new dose metric [5]. Since the APD is immeasurable in practice due to discrepancies in tissue properties, variability in geometric configuration of the skin and other individual-specific biologically-significant properties, as well as for the ethical reasons, the incident power density (IPD) is instead used as the reference level [6]. In this paper, we are concerned with the evaluation of the IPD, or, as later stated, free space approximation of the APD on the irradiated area of human skin in a close proximity of a half-wave dipole operating in the 5G frequency spectrum.

Since the mmWave spectrum covers frequencies well beyond the ones covered in all previous generations of telecommunication technologies, simulations of radiated EMFs and the interaction with human tissue, especially in near-field conditions, must be approached with increased caution. Given that the computation of gradients is ubiquitous in the computational electromagnetic dosimetry, instead of performing numerical differentiation, this paper showcases automatic differentiation in assessment of the APD. Generally, automatic differentiation is defined as the set of algorithmic techniques to evaluate the derivative of a differentiable function defined programmatically to its numerical precision [7]. Automatic differentiation is widely used in many applied sciences: computational fluid dynamics [8], inverse electromagnetic simulations [9], optimal control [10], molecular dynamics and differentiable physics in general [11], and overall differentiable programming [12]. Differentiable programming has found use in a wide variety of areas, particularly in scientific computing [13] and machine learning, i.e., deep learning in neural networks [14]. To the best of authors' knowledge, this work pioneers the use of automatic differentiation to simulate phenomena that are encountered in the electromagnetic dosimetry. Even though, there are various libraries and frameworks that allow a user to seamlessly deploy automatic differentiation principles to a differentiable problem at hand, all examples[1] in this paper are implemented by using JAX, Python based, extensible system for transforming numerical functions [15]. In its core, JAX is an extensible system for composable function transformations, where the two most prominent transformations are automatic differentiation of native Python and NumPy [16] functions and just-in-time compilation powered by XLA (Accelerated Linear Algebra)[2].

[1]To enable seamless reproduction of presented results in the paper, the associated code-base is open-sourced and available at https://github.com/antelk/ipd-autodiff.

[2]https://www.tensorflow.org/xla

The paper is outlined as follows. The overview of automatic differentiation along with the motivating example on how, when and why automatic differentiation should be employed is given in Section II. Furthermore, Section III outlines the calculation of radiated EMFs from the Hertz half-wave dipole placed in the immediate vicinity of human tissue. The assessment of the APD is obtained from field equations by utilizing automatic differentiation of the Green function. In Section IV, the analysis of the use of automatic differentiation as an adequate substitute for numerical differentiation in electromagnetic dosimetry is given; numerical and automatic differentiation are compared in terms of accuracy (comprehensive evaluation of the total numerical error in various scenarios) and execution speed. Finally, the conclusion and closing remarks are given in Section V.

II. Automatic Differentiation

Numerical differentiation is a finite difference approximation of the limit definition of a derivative. For any scalar-valued function $f : \mathbb{R}^n \to \mathbb{R}$, the derivative at a point x is defined by the limit as follows:

$$\frac{df(x)}{dx} = \lim_{\delta \to 0} \frac{f(x+\delta) - f(x)}{\delta} \tag{1}$$

where δ is the limit of difference approaching zero. Instead, if δ is a non-zero and fixed value, it is interpreted as the step size of a finite difference. Difference quotient approximates the derivative by measuring the average rate of change of a function over an interval of length δ:

$$\frac{df(x)}{dx} \approx \frac{f(x+\delta) - f(x)}{\delta} \tag{2}$$

where eq. (2) is defined as a forward finite difference. Assuming that f is twice-differentiable, a more accurate approximation can be utilized:

$$\frac{df(x)}{dx} \approx \frac{f(x+\delta/2) - f(x-\delta/2)}{\delta} \tag{3}$$

and is referred to as a central finite difference. Analogously, higher order derivative approximations utilizing a central finite difference are obtained in a recursive manner:

$$\begin{aligned} \frac{df^2(x)}{dx^2} &\approx \frac{\frac{f(x+\delta)-f(x)}{\delta} - \frac{f(x)-f(x-\delta)}{\delta}}{\delta} \\ &\approx \frac{f(x+\delta) - 2f(x) + f(x-\delta)}{\delta^2} \end{aligned} \tag{4}$$

which is proved by expanding the expression in Taylor series, available elsewhere, e.g., in [17].

Central finite difference yields the total numerical error of $\mathcal{O}(\delta^2)$ instead of $\mathcal{O}(\delta)$, associated with a forward (as well as a backward) finite difference approximation. The total numerical error is the accumulated error quantity directly dependant on the ill-conditioned implementation of the difference quotient formula. The error resulting from the truncation is a consequence of δ being a non-zero value. Round-off error, on the other hand, occurs because of the finite machine numerical precision and floating-point arithmetic used to represent real values, but again arises from the very choice of δ. Truncation error scales proportionally with a power of δ, while round-off error is inversely proportional to a power of δ. To get a further grasp on the difficulty defining the appropriate step size and the numerical error as the main weakness of a central finite difference approximation, let's consider an example of a single-valued periodic function:

$$f(x) = \sin(\sin(x)), \tag{5}$$

with the analytic expression for its 1^{st} order derivative:

$$\frac{df(x)}{dx} = 2\cos(2x)\cos(\sin(2x)), \tag{6}$$

and the 2^{nd} order derivative:

$$\begin{aligned} \frac{d^2 f(x)}{dx^2} = -4 \cdot \Big(&\sin\big(\sin(2x)\big)\cos^2(2x) \\ &+ \sin(2x)\cos\big(\sin(2x)\big)\Big). \end{aligned} \tag{7}$$

Figure 1 shows the total numerical error, truncation dominant for large values of δ and round-off dominant for small values of δ. Even though there are ways to circumvent round-off

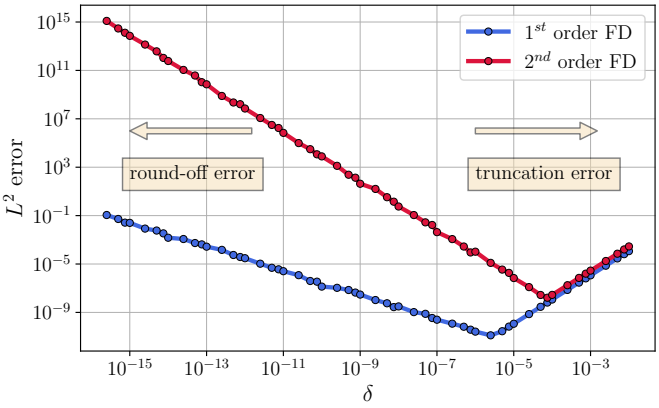

Fig. 1. Truncation and round-off error for the 1^{st} and the 2^{nd} order derivatives approximated via a central finite difference (FD) for a function, f, given in eq. (5). Errors are calculated as the L^2-norm of the difference between FD approximations and the actual values obtained via analytical expressions in eq. (6) and eq. (7) over the range of 21 value for $x \in [-1, 1]$.

error by choosing the optimal step size as the cube-root of machine epsilon [18] and by employing complex step approximation [19], it is fairly obvious that truncation error is heavily dependent on a problem at hand.

Another approach is the use of symbolic differentiation instead of numerical differentiation. Standard derivative rules are applied computationally to a closed-form expression of a function, transforming it into the derivative of interest. This approach avoids numerical instabilities and the accumulated numerical error by allowing the exact computation of derivatives up to machine precision. Unlike numerical differentiation, symbolic differentiation does not suffer from the curse of dimensionality. In order to obtain the Jacobian matrix, J, for any differentiable function $f : \mathbb{R}^n \to \mathbb{R}^m$, numerical differentiation requires $\mathcal{O}(nm)$ computations of the function f itself, while symbolic differentiation requires

$\mathcal{O}(n)$ vectorized computations. However, it comes with a set of its own difficulties. Firstly, derivative expression swell is a common occurrence, where due to applied derivative rules, the derivative expression may be substantially larger than the original function. Moreover, symbolic differentiation requires the closed-form expression of the original function, which means that it is virtually impossible to exploit such an approach for dosimetry problems, often computationally realized by using the control flow mechanism.

By operating directly on the computational description of the problem of interest, automatic differentiation achieves the same numerical precision as symbolic differentiation, producing the actual numerical value rather than the expression of a derivative [7]. Automatic differentiation operates by breaking the necessary computation into a sequence of primitive operations with derivatives known in advance. The chain rule is then applied to the composition of primitive derivatives to obtain the final derivative value. The two modes of automatic differentiation are known as forward and backward accumulation. Forward accumulation requires fixing the input independent variable with respect to which differentiation is performed and computes value-derivative pairs of each primitive operation comprising the function expression. A forward pass yields a function value (or values if multi-output function is considered instead) along with the derivative of interest for the specific input value. In general circumstances, for a function with multiple input independent variables, $f : \mathcal{R}^n \rightarrow \mathcal{R}^m$, each forward pass results in a partial derivative of a single input variable i.e., a single corresponding column of the Jacobian matrix. Computing the entire Jacobian matrix, in this case, would require n passes. For a situation where $n \ll m$, forward accumulation is preferred, otherwise backward accumulation should be considered. Backward accumulation, also commonly denoted as the reverse mode automatic differentiation, propagates derivatives backward from the output. The process begins by forward passing input variables through the function expression, this time computing values of the expression chain and capturing dependencies into the computational graph, storing both in memory. The second part of the process is the computation of the derivatives by propagating adjoints starting from the output, in a reverse manner. Finally, partial derivatives with respect to each input i.e., each row of the associated Jacobian matrix, are obtained in a single execution of backward accumulation, a perfect scenario for a situation where $m \ll n$. Automatic differentiation in comparison to numerical differentiation by using the simple toy example given in eq. (5) is visually presented in fig. 2. The total numerical error, defined as the L^2-norm difference between the actual derivative values computed via analytical expressions in eq. (6) and eq. (7), corresponding to the 1^{st} and the 2^{nd} order derivative, respectively, and approximated values for $x \in [-1, 1]$ is given in table I.

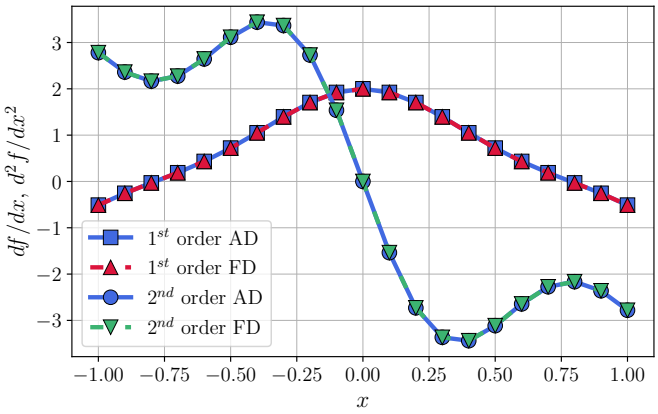

Fig. 2. Automatic differentiation (AD) and a central finite difference (FD) for the 1^{st} and 2^{nd} order derivative of eq. (5). The evaluation of the total numerical error for both AD and FD is given in table I.

TABLE I
EVALUATION OF THE TOTAL NUMERICAL ERROR

Differentiation	Order	RMSE
Numerical	1^{st}	$1.16 \cdot 10^{-4}$
	2^{nd}	$2.84 \cdot 10^{-4}$
Automatic	1^{st}	0.0
	2^{nd}	0.0

III. RADIO-FREQUENCY TRANSMITTED EMFS RADIATED BY A HALF-WAVE HERTZ DIPOLE

Consider a canonical setup where a center-fed half-wave Hertz dipole is placed near the planar model of human tissue defined by the surface of area A. Schematic of the geometry can be visually explored in fig. 3.

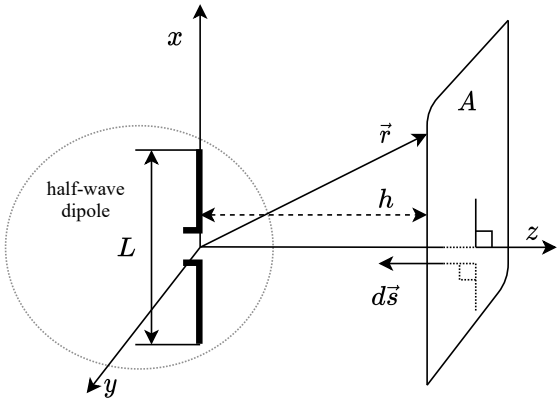

Fig. 3. A center-fed half-wave Hertz dipole in free space. Area, A, represents the effective integration surface of the tissue on a distance h from the source.

Current distribution along the dipole is governed by the Pocklington integro-differential equation. Pocklington equation can be derived by enforcing the interface conditions for

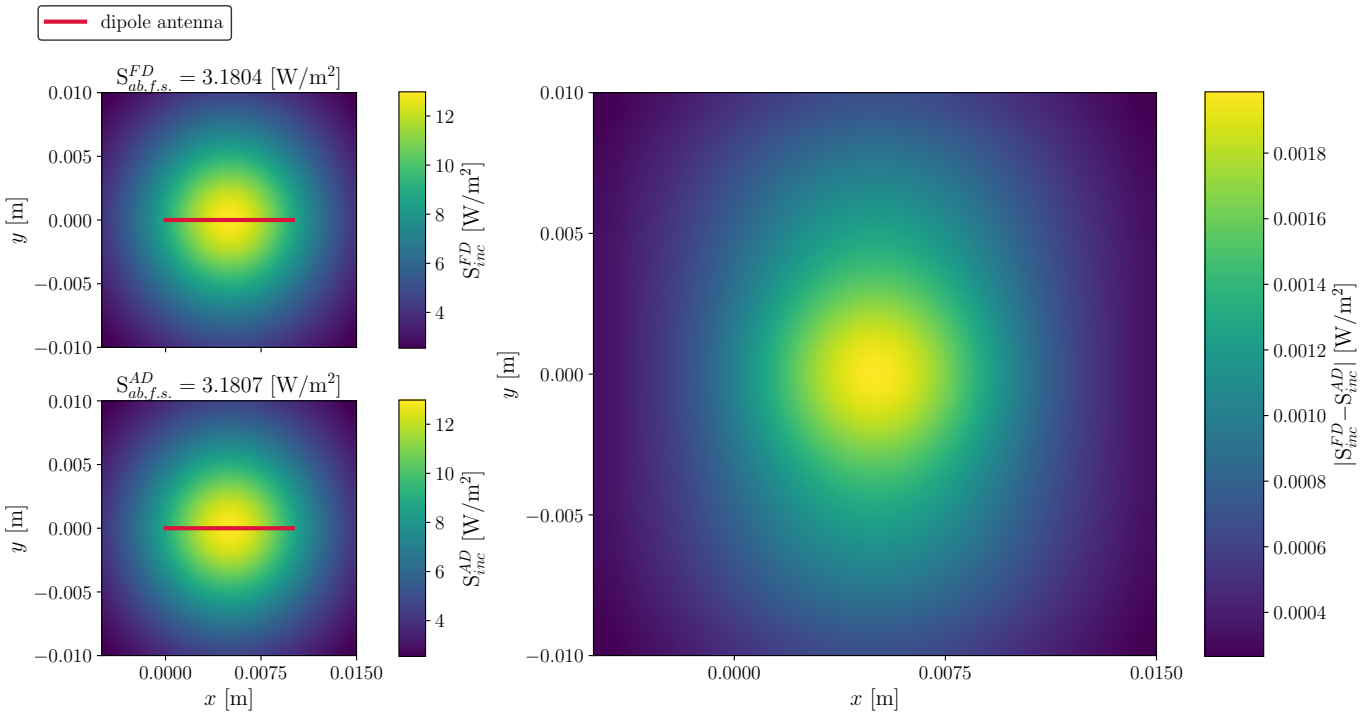

Fig. 4. Comparison between the power density calculated by automatic (AD) and numerical differentiation (a finite central difference method, FD), respectively. The panel on the right shows the absolute difference between the two approaches. Averaging area, A equals to 4 cm^2, distance between the dipole and the averaging area, h, is 10 mm and operating frequency of the dipole, f, is set to 15 GHz.

the tangential components of the electric field at the perfectly conducting surface, and is given as follows [17]:

$$E_x^{exc} = j\omega\frac{\mu_0}{4\pi}\int_{-L/2}^{L/2} I(x')g(x,y,z,x')dx' - \frac{1}{j4\pi\omega\epsilon_0}\frac{\partial}{\partial x}\int_{-L/2}^{L/2}\frac{\partial I(x')}{\partial x'}g(x,y,z,x')dx' \tag{8}$$

where $I(x')$ is the current distribution and $g(x,y,z,x')$ is the Green function in free space:

$$g(x,y,z,x') = \frac{\mathrm{e}^{-jkR}}{R} \tag{9}$$

with R representing the Euclidian distance from the source point, x', to the observation point, (x,y,z), i.e., the magnitude of the position vector $\vec{r}$. Other parameters are, as follows, angular frequency, ω, magnetic permeability of free space, μ_0, and permittivity of free space, ϵ_0. Additionally, in the Green function, k stands for the wave number. By setting the operating frequency, f, angular frequency. ω, and the length of the dipole, L, are adjusted accordingly. It is important to emphasize that the solution of eq. (8) is carried out by means of Galerkin-Bubnov scheme of the indirect boundary element method by using 51 wire segments (boundary elements along the dipole) and setting the radius of the dipole to $1/10$ of the length of a single segment as if it was a matter of free space conditions. The middle segment is driven by a voltage source set to 1 V. Once the current distribution is obtained, electric field equations arise from the boundary element formalism as follows:

$$E_x = \frac{1}{j4\pi\omega\epsilon_0}\left(\int_{-L/2}^{L/2}\frac{\partial I(x')}{\partial x'}\frac{\partial g(x,y,z,x')}{\partial x}dx' - k^2\int_{-L/2}^{L/2} I(x')g(x,y,z)dx'\right) \tag{10}$$

$$E_y = \frac{1}{j4\pi\omega\epsilon_0}\int_{-L/2}^{L/2}\frac{\partial I(x')}{\partial x'}\frac{\partial g(x,y,z,x')}{\partial y}dx' \tag{11}$$

$$E_z = \frac{1}{j4\pi\omega\epsilon_0}\int_{-L/2}^{L/2}\frac{\partial I(x')}{\partial x'}\frac{\partial g(x,y,z,x')}{\partial z}dx' \tag{12}$$

while magnetic field equations are derived from the Maxwell–Faraday equation:

$$H_y = \frac{1}{4\pi}\int_{-L/2}^{L/2} I(x')\frac{\partial g(x,y,z,x')}{\partial z}dx' \tag{13}$$

$$H_z = -\frac{1}{4\pi}\int_{-L/2}^{L/2} I(x')\frac{\partial g(x,y,z,x')}{\partial y}dx' \tag{14}$$

Consider now a 5G mobile communication device in a close proximity of human tissue. Absorbed power density (APD) is used as the basic restriction for the human exposure to EMFs radiated from a device. It is defined at the body surface, averaged over the tissue area of interest, A, and is written as follows:

$$S_{ab} = \frac{1}{2A}\iint_A \Re[\vec{S}]d\vec{s} \tag{15}$$

where Poynting vector, $\vec{S} = \vec{E} \times \vec{H}^*$, yields a direction of the electromagnetic wave propagation and stems from the Poynting theorem, representing a general conservation law for the energy stored in the electric and the magnetic field. Since both $\vec{E}$ and $\vec{H}$ are incident, rather than absorbed, eq. (15) represents free space approximation of the APD. Variable vector, $d\vec{s}$, has its direction normal to the integral area A on the body surface, as shown in fig. 3, thus leading to the simplification of eq. (15):

$$S_{ab} = \frac{1}{2A} \iint_A \Re[E_x H_y^*] d\vec{s} \tag{16}$$

In order to calculate electromagnetic vector field and, subsequently, the power density distribution and free space approximation of the APD, gradients of the Green function must be evaluated for each observation point multiple times. The relationship of the accuracy of the power distribution, obtained either by utilizing automatic or numerical differentiation, on the observed surface is shown in fig. 4. One can clearly see that, assuming machine precision of automatic differentiation, it has a better overall accuracy compared to numerical differentiation. In this case, the level of accuracy is visible in the fourth decimal place of the averaged power density.

IV. Discussion

The absolute difference between the two equally configured simulations, differing solely in the way the gradients of the Green function are evaluated, with the final output visualized in fig. 4, does not seem notable at first. This difference becomes substantial once the configuration of the simulation starts to change, in a situation where the step size in numerical differentiation is not adjusted. Superiority of automatic over numerical differentiation is illustrated in fig. 5. Namely, the

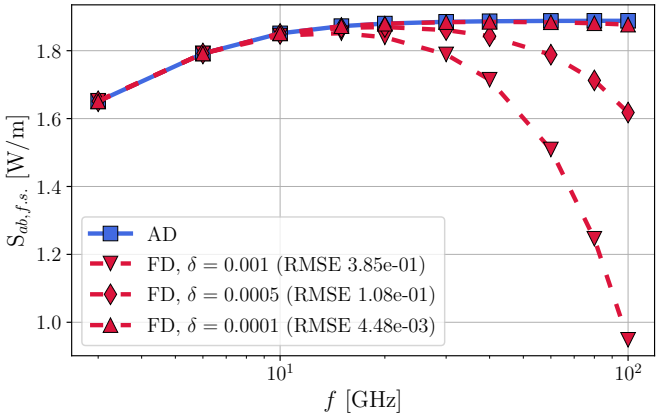

Fig. 5. Comprehensive simulation for the range of frequencies between 3 and 100 GHz. Averaging area, A, equals to 4 cm, distance between the dipole and the averaging area, h, is 15 mm.

final result (caused by the inherent issue of truncation error, unavoidable when utilizing numerical differentiation) reaches an error of more than 50 percent of the actual value for the worst case scenario.

Additional advantage of using automatic differentiation is considerable speedup in execution time. By using backward mode accumulation, a single row of the Jacobian matrix is calculated in a single execution. Within numerical differentiation procedure, one has to evaluate a function of interest at least two times per execution for each value of the input independent variable with regard to which the function is derived. For the simulation outlined in Section III, where the final results are shown in fig. 4, the time needed for the calculation of all necessary gradients of the Green function using numerical differentiation is 7.28 s $\pm$0.44 s of 7 runs in total. On the other hand, automatic differentiation with JAX is able to perform the computation of gradients in 250 ms $\pm$1.65 ms of 7 runs in total. Thus, the overall speedup is 29.13 times $\pm$0.33 and the cumulative distribution of speedups for each combination of 7×7 runs is shown in fig. 6.

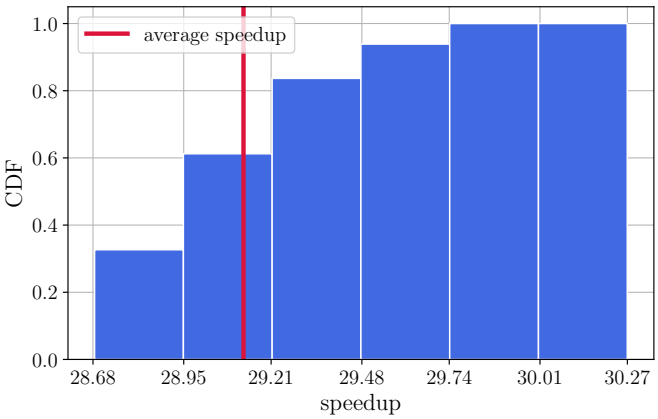

Fig. 6. Cumulative distribution function of speedups defined as the ratio between execution times needed to calculate all gradients associated with the simulation corresponding to fig. 4 by using automatic differentiation and numerical differentiation, respectively.

V. Conclusion

This paper deals with the application of automatic differentiation in computational electromagnetic dosimetry. Automatic differentiation achieves a twofold improvement in terms of accuracy and execution time over numerical differentiation approach. Illustrative examples of the assessment of the APD on the planar model of human tissue have been presented for a variety of frequencies in mmWave range, where automatic differentiation has been proven to be superior over numerical differentiation. Future work will likely deal with more realistic human exposure scenarios where automatic differentiation guarantees machine precision irrespective of model geometry, a common obstacle when approximating derivatives numerically.

Acknowledgment

This research has been funded by DATACROSS project of The Centre of Research Excellence for Data Science and Advanced Cooperative Systems (CRE ACROSS-DataScience).

REFERENCES

[1] International Commission on Non-Ionizing Radiation Protection (ICNIRP), "Guidelines for limiting exposure to electromagnetic fields (100 kHz to 300 GHz)," *Health Physics*, vol. 118, pp. 483–524, 2020. [Online]. Available: https://doi.org/10.1097/HP.0000000000001210

[2] "IEEE standard for safety levels with respect to human exposure to electric, magnetic, and electromagnetic fields, 0 Hz to 300 GHz," *IEEE Std C95.1-2019 (Revision of IEEE Std C95.1-2005/ Incorporates IEEE Std C95.1-2019/Cor 1-2019)*, pp. 1–312, 2019. [Online]. Available: https://doi.org/10.1109/IEEESTD.2019.8859679

[3] T. Wu, T. S. Rappaport, and C. M. Collins, "Safe for generations to come: Considerations of safety for millimeter waves in wireless communications," *IEEE Microwave Magazine*, vol. 16, no. 2, pp. 65–84, 2015. [Online]. Available: https://doi.org/10.1109/MMM.2014.2377587

[4] D. Funahashi, T. Ito, A. Hirata, T. Iyama, and T. Onishi, "Averaging area of incident power density for human exposure from patch antenna arrays," *IEICE Transactions on Electronics*, vol. E101.C, no. 8, pp. 644–646, 2018. [Online]. Available: https://doi.org/10.1587/transele.E101.C.644

[5] A. Hirata, "Review on human dosimetry for radio-frequency exposure above 6 GHz - International exposure standards," *2018 Asia-Pacific Microwave Conference*, pp. 681–683, 2018. [Online]. Available: https://doi.org/10.23919/APMC.2018.8617491

[6] A. Hirata, D. Funahashi, and S. Kodera, "Setting exposure guidelines and product safety standards for radio-frequency exposure at frequencies above 6 ghz: brief review," *Annals of Telecommunications*, vol. 74, pp. 17–24, 2019. [Online]. Available: https://doi.org/10.1007/s12243-018-0683-y

[7] A. G. Baydin, B. A. Pearlmutter, A. A. Radul, and J. M. Siskind, "Automatic differentiation in machine learning: a survey," *Journal of Machine Learning Research*, vol. 18, no. 153, pp. 1–43, 2018. [Online]. Available: https://www.jmlr.org/papers/v18/17-468.html

[8] C. Bischof, G. Corliss, L. Green, A. Griewank, K. Haigler, and P. Newman, "Automatic differentiation of advanced cfd codes for multidisciplinary design," *Computing Systems in Engineering*, vol. 3, no. 6, pp. 625–637, 1992. [Online]. Available: https://doi.org/10.1016/0956-0521(92)90014-A

[9] T. Hughes, I. Williamson, M. Minkov, and S. Fan, "Forward-mode differentiation of Maxwell's equations," *ACS Photonics*, vol. 6, pp. 3010—-3016, 2019. [Online]. Available: https://doi.org/10.1021/acsphotonics.9b01238

[10] A. Walther, "Automatic differentiation of explicit Runge-Kutta methods for optimal control," *Computational Optimization and Applications*, vol. 36, pp. 83–108, 2007. [Online]. Available: https://doi.org/10.1007/s10589-006-0397-3

[11] S. Schoenholz and E. D. Cubuk, "JAX MD: A framework for differentiable physics," *Advances in Neural Information Processing Systems*, vol. 33, pp. 11 428–11 441, 2020. [Online]. Available: https://proceedings.neurips.cc/paper/2020/file/83d3d4b6c9579515e1679aca8cbc8033-Paper.pdf

[12] M. Innes, A. Edelman, K. Fischer, C. Rackauckas, E. Saba, V. B. Shah, and W. Tebbutt, "A differentiable programming system to bridge machine learning and scientific computing," 2019. [Online]. Available: https://arxiv.org/abs/1907.07587v2

[13] C. Rackauckas, Y. Ma, J. Martensen, C. Warner, K. Zubov, R. Supekar, D. Skinner, A. Ramadhan, and A. Edelman, "Universal differential equations for scientific machine learning," *Research Square*, 2020. [Online]. Available: https://doi.org/10.21203/rs.3.rs-55125/v1

[14] J. Schmidhuber, "Deep learning in neural networks: An overview," *Neural Networks*, vol. 61, pp. 85–117, 2015. [Online]. Available: https://doi.org/10.1016/j.neunet.2014.09.003

[15] J. Bradbury, R. Frostig, P. Hawkins, M. J. Johnson, C. Leary, D. Maclaurin, G. Necula, A. Paszke, J. VanderPlas, S. Wanderman-Milne, and Q. Zhang, "JAX: composable transformations of Python+NumPy programs," 2018. [Online]. Available: http://github.com/google/jax

[16] C. R. Harris, K. J. Millman, S. J. van der Walt, R. Gommers, P. Virtanen, D. Cournapeau, E. Wieser, J. Taylor, S. Berg, N. J. Smith, R. Kern, M. Picus, S. Hoyer, M. H. van Kerkwijk, M. Bett, A. Haldane, J. F. del Río, M. Wiebe, P. Peterson, P. Gérard-Marchant, K. Sheppard, T. Reddy, W. Weckesser, H. Abbasi, C. Gohlke, and T. E. Oliphant, "Array programming with NumPy," *Nature*, vol. 585, no. 7825, pp. 357–362, 2020. [Online]. Available: https://doi.org/10.1038/s41586-020-2649-2

[17] D. Poljak, *Advanced Modeling in Computational Electromagnetic Compatibility*. Wiley, 2006. [Online]. Available: https://doi.org/10.1002/0470116889

[18] J. Nash, *Compact Numerical Methods for Computers: Linear Algebra and Function Minimisation*. Routledge 2nd edition, 1979. [Online]. Available: https://doi.org/10.1201/9781315139784

[19] K.-L. Lai and J. L. Crassidis, "Extensions of the first and second complex-step derivative approximations," *Journal of Computational and Applied Mathematics*, vol. 219, no. 1, pp. 276–293, 2008. [Online]. Available: https://doi.org/10.1016/j.cam.2007.07.026